STM JOURNALS

Journal of
Polymer & Composites

ISSN: 2321-2810 (Online)
ISSN: 2321-8525 (Print)
Volume 14, Issue 2, 2026
DOI (Journal): 10.37591/JoPC

https://journals.stmjournals.com/jopc

Research JoPC

# Combustion Synthesis and Comprehensive Characterization of Pure and Ni-Doped $CuFe_2O_4$ Nanoparticles for Functional Composite Applications

A. Selvaraj[1], M. Sundararajan[2], S. Nandhini[3], S. Yuvaraj[4,*], Chandra Sekhar Dash[5], Jagadeesh Kumar Alagarasan[6], Arun Thirumurugan[7], Gabriela Sandoval Hevia[8], Tejaswi Ashok Hegde[9], P Aji Udhaya[10]

***Abstract***

*The $CuFe_{2-x}Ni_xO_4$ (x = 0, 0.1, 0.3, and 0.5) nanoparticles were synthesized using a combustion method and comprehensively characterized to understand their suitability for polymer-based composite applications. X-ray diffraction confirmed the formation of a single-phase spinel ferrite structure with crystallite sizes of 20–30 nm. Energy-dispersive X-ray spectroscopy verified the successful incorporation of Ni ions into the $CuFe_2O_4$ lattice, while FE-SEM analysis revealed uniformly dispersed nanoscale particles desirable for composite reinforcement. Optical characterization showed a gradual reduction in band gap energy from 1.81 to 1.75 eV with increasing Ni content, indicating enhanced electronic interactions that can contribute to improved functional performance in polymer matrices. FT-IR spectra further validated the structural stability of the Ni-substituted ferrites through characteristic metal–oxygen stretching vibrations. The tunable structural and optical properties of $CuFe_{2-x}Ni_xO_4$ nanoparticles highlight their potential as promising fillers for multifunctional polymer and hybrid composite materials.*

***Author for Correspondence**
S. Yuvaraj

[1]Assistant Professor, Department of Mathematics, Vel Tech Rangarajan Dr. Sagunthala R&D Institute of Science and Technology, Vel Nagar, Avadi, Chennai, Tamil Nadu, India
[2]Assistant Professor, Department of Physics, Paavendhar College of Arts & Science, M.V. South, Thalaivasal, Salem, Tamil Nadu, India
[3,4]Research Scholar, Department of Physics, Vel Tech Rangarajan Dr. Sagunthala R&D Institute of Science and Technology, Vel Nagar, Avadi, Chennai, Tamil Nadu, India
[5]Associate Professor, Department of Electronics and Communication Engineering, Centurion University of Technology and Management, Odisha, Bhubaneswar, India
[6]Associate Professor, Department of Chemistry, Faculty of Science, Technology and Architecture (FoSTA), Manipal University Jaipur, Rajasthan, India
[7]Assistant Professor, Department of Chemistry, Vallenar Campus, University of Atacama, 105 Costanera, Avenue Vallenar 1612178, Chile
[8]Associate Professor, Department of Chemistry, Metropolitan Technological University, Santiago, 7800002, Chile
[9]Assistant Professor, Department of Physics, Hindustan Institute of Technology and Science, Chennai, Tamil nadu, India
[10]Assistant Professor, Department of Physics, Holy Cross College, Nagercoil, Tamil Nadu, India

Received Date: December 22, 2025
Accepted Date: January 09, 2026
Published Date: February 11, 2026

**Citation:** A. Selvaraj, M. Sundararajan, S. Nandhini3, S. Yuvaraj, Chandra Sekhar Dash, Jagadeesh Kumar Alagarasan, Arun Thirumurugan, Gabriela Sandoval Hevia, Tejaswi Ashok Hegde, P Aji Udhaya. Combustion Synthesis and Comprehensive Characterization of Pure and Ni-Doped $CuFe_2O_4$ Nanoparticles for Functional Composite Applications. Journal of Polymer & Composites. 2026; 14(2): 1–11p.

**Keywords**: $CuFe_2O_4$, combustion method, structural, band gap, composite applications

## INTRODUCTION

Magnetic nanoparticles, particularly spinel ferrite nanomaterials, have gained significant attention due to their unique physicochemical behavior and potential integration into advanced composite systems. Owing to their nanoscale dimensions, these ferrites exhibit properties distinct from their bulk counterparts, including single-domain magnetic behavior, enhanced surface activity, and quantum size effects [1-3]. Such characteristics make them attractive candidates for incorporation into polymer matrices to develop multifunctional composites with improved magnetic [4,5], electronic [6], and dielectric [7] responses.

© STM Journals 2026. All Rights Reserved 

Spinel ferrites with the general formula $MFe_2O_4$ represent an important class of soft magnetic oxides with tunable structural and functional characteristics. Their adjustable cation distribution and strong structure–property correlations make them highly suitable for engineering polymer nanocomposites used in energy storage, environmental remediation, electromagnetic shielding, and sensing technologies. Among them, $CuFe_2O_4$ is a promising material due to its stable spinel structure, room-temperature magnetic activity, and compatibility with various composite fabrication routes. The distribution of $Fe^{3+}$ ions at octahedral (B) sites and $Cu^{2+}$ ions at tetrahedral (A) sites [8,9] influences its magnetic, optical, and electrical behavior, enabling targeted modification for composite applications.

Doping strategies have been widely explored to overcome limitations such as restricted electrical conductivity, magnetic softness, and limited visible-light absorption. Incorporation of metal ions such as $Mg^{2+}$, $Mn^{2+}$, $Ca^{2+}$, or $Ni^{2+}$ has been shown to enhance the functional performance of $CuFe_2O_4$ nanoparticles, leading to better dielectric characteristics, improved magnetization, reduced crystallite size, and enhanced photocatalytic activity [10,11]. These tunable properties are especially advantageous for polymer-based nanocomposites where filler–matrix interactions govern the overall dielectric, optical, and mechanical behavior [12,13].

Nickel substitution in copper ferrites, in particular, has demonstrated improved charge mobility, structural refinement, and enhanced soft magnetic characteristics, making Ni-doped ferrites suitable for use in polymeric composites for electromagnetic interference (EMI) shielding, microwave absorption, optoelectronics, and catalytic systems [14]. The ability to tailor dielectric losses, electrical resistivity, and magnetic response through controlled doping further broadens their application potential in multifunctional composite materials [15,16].

In this work, Ni-doped $CuFe_2O_4$ nanoparticles were synthesized via a combustion method and systematically analyzed to assess the influence of Ni incorporation on their structural, morphological, and functional characteristics. Special emphasis is placed on understanding how compositional modification and thermal treatment contribute to property enhancement. By establishing the relationship between Ni substitution and resulting material behavior, this study highlights the suitability of $CuFe_{2-x}Ni_xO_4$ nanoparticles as efficient fillers for advanced polymer and hybrid composite systems designed for next-generation technological applications.

## EXPERIMENTAL

### Materials

High quality chemicals (≥99%), including $Ni(NO_3)_2{\cdot}6H_2O$, $C_6H_{14}N_4O_2$ (L-arginine), $Fe(NO_3)_3{\cdot}9H_2O$, and $Cu(NO_3)_2{\cdot}3H_2O$, were used exactly as supplied, without further purification. In order to prepare each sample, deionized water was used.

### Synthesis of $CuFe_{2-x}Ni_xO_4(0\leq x\leq 0.5)$ Nanoparticles

$CuFe_{2-x}Ni_xO_4$ ($0 \leq x \leq 0.5$) nanoparticles were synthesized by dissolving stoichiometric amounts of $Ni(NO_3)_2{\cdot}6H_2O$, $C_6H_{14}N_4O_2$ (L-arginine), $Fe(NO_3)_3{\cdot}9H_2O$, and $Cu(NO_3)_2{\cdot}3H_2O$ in deionized water. The resulting solution was mechanically agitated continuously at room temperature for one hour to achieve homogeneity. In this process, $C_6H_{14}N_4O_2$ functioned as the fuel with a fuel-to-oxidizer ratio of 1, while the metal nitrates served as oxidizers.

The homogeneous mixture was then heated to 90°C for 10 minutes in a hot air oven, initiating the combustion process. The process involved a series of steps, including sequential boiling, dehydration, decay, gas development, and spontaneous burst, ultimately forming solid, fluffy $CuFe_{2-x}Ni_xO_4$ nanoparticles [17]. The resulting samples were subsequently calcined for 90 minutes at 800°C, with a regulated heating rate of 5°C per minute [18]. The synthesized nanoparticles were labelled as follows:a: $CuFe_2O_4$b: $CuFe_{1.9}Ni_{0.1}O_4$c: $CuFe_{1.7}Ni_{0.3}O_4$d: $CuFe_{1.5}Ni_{0.5}O_4$.

© STM Journals 2026. All Rights Reserved 

### Characterization Techniques

Using different characterization techniques, the optical, magnetic, morphological, and structural characteristics of $CuFe_{2-x}Ni_xO_4$ (x = 0, 0.1, 0.3, and 0.5) were investigated in detail. The size of the crystallites and phase formation were verified by X-ray diffraction (XRD). Energy-dispersive X-ray spectroscopy (EDX) and field emission scanning electron microscopy (FE-SEM) were used to analyse the particle's morphology and elemental makeup. Fourier-transform infrared (FTIR) spectroscopy was used to detect vibrational modes and functional groups, while UV-Vis spectroscopy was used to assess optical characteristics, including band gap analysis. These characterization techniques collectively enabled a detailed assessment of the material properties relevant for advanced composite and functional applications.

## RESULT AND DISCUSSION

### Powder X-Ray Diffraction Analysis

The crystalline nature of the $CuFe_{2-x}Ni_xO_4$ (x = 0, 0.1, 0.3, and 0.5) nanoparticles is confirmed by their X-ray diffraction (XRD) spectra, which is shown in Figure 1. The Bragg reflection planes (220), (311), (400), (422), (511), (440), (533) and (622), respectively, are represented by the distinct peaks in the diffractograms at 2θ values of 30.09°, 35.65°, 43.02°, 53.78°, 57.50°, 62.83°, and 74. 20°.According to the standard JCPDS card number77-0010, these reflections match. Further, the $Fe_2O_3$ peaks are also found that the 2-theta value 24.37˚, 33.37˚, 37.36˚, 38.93˚, 40.92˚, 43.48˚, 48.88˚, 49.61˚, 50.87˚, 66.38˚, 68.16˚ and 72.13˚ respectively. The formation of a cubic spinel structure with the Fd3m space group was confirmed [18, 21].

The average crystallite size (L) can be computed using the Debye-Scherrer equation (Eq. 1) was used along with using the reference plane of the (311) reflection.

$$L = \frac{0.89\lambda}{\beta \cos\theta} \quad (1)$$

where θ is the Bragg angle, β is the full width at half maximum (FWHM) of the (311) peak in radians, λ is the wavelength of the X-ray source, L is the crystallite size, and K is the shape factor [19].
The estimated average crystallite size, using this equation, was between 20 nm (x = 0) and 30 nm (x = 0.5).

In Figure 2, the bottom curve shows the difference between the experimental and intended XRD patterns. Rietveld refinement verified that the synthesized samples had a spinel-type crystal structure.

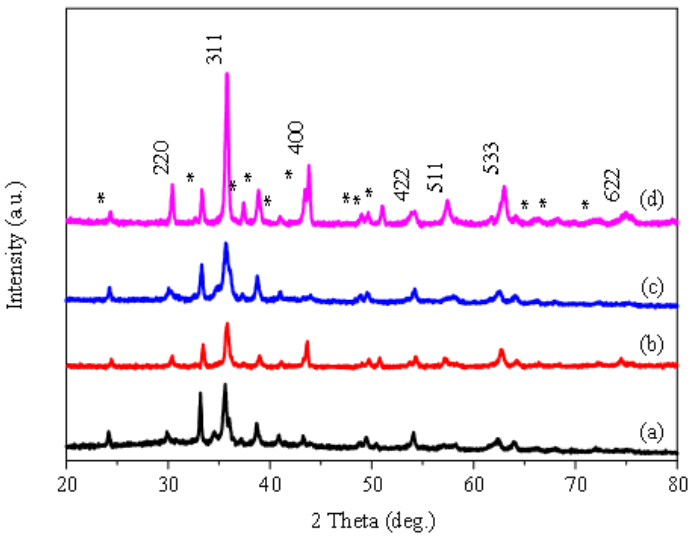


**Figure 1.** XRD patterns of $CuFe_{2-x}Ni_xO_4$ (x = 0, 0.1, 0.3 & 0.5) nanoparticles.

© STM Journals 2026. All Rights Reserved 

The lattice parameter (a) for $CuFe_{2-x}Ni_xO_4(0 \leq x \leq 0.5)$ was computed using Eq. 2:

$$a = d_{hkl}\sqrt{(h^2 + k^2 + l^2)} \quad (2)$$

where (h, k, l) are the Miller indices that correspond to the particular crystallographic planes, and $d_{hkl}$ is the interplanar spacing [20].

The calculated lattice parameters were 8.320 Å for $CuFe_2O_4$ and 8.317 Å, 8.313 Å, and 8.310 Å for $CuFe_{2-x}Ni_xO_4$ with x = 0.1, 0.3, and 0.5, respectively.

The progressive decrease in the lattice parameter with increasing $Ni^{2+}$ substitution is attributed to the smaller ionic radius of $Ni^{2+}$ (0.69 Å) compared to $Cu^{2+}$ (0.77 Å) [21]. This systematic contraction of the unit cell further confirms the successful incorporation of $Ni^{2+}$ ions into the $CuFe_2O_4$ lattice. The structural parameters summarized in Table 1 clearly support the formation of a cubic spinel phase for all $CuFe_{2-x}Ni_xO_4$ $(0 \leq x \leq 0.5)$ compositions.

The Rietveld refinement analysis (Table 2) was carried out on all samples of $CuFe_{2-x}Ni_xO_4$ (x = 0, 0.1, 0.3, and 0.5) nanoparticles using the FULLPROF [22] programme to investigate its structural properties. The refinements were performed within the *Fd3m* space group. As depicted in Figure 2., the observed XRD patterns align well with the calculated ones, with no additional phases detected.

The goodness-of-fit index (*S*), defined as

$$S = \frac{R_{wp}}{R_e}$$

where the weighted profile reliability factor is represented by $R_{wp}$, and the expected weighted profile reliability factor by $R_e$. Rietveld refinement factors of $CuFe_{2-x}Ni_xO_4$ $(0 \leq x \leq 0.5)$ samples are tabulated in table 1 and the goodness-of-fit index (*S*) of all the four samples are approximately 1. This indicates a strong agreement between the observed and calculated profiles, further validating the accuracy of the refinements and the excellent fit of the data.

**Field Emission Scanning Electron Microscopy (FE-SEM) Analysis**

Field-emission scanning electron microscopy (FE-SEM) was used to investigate the surface morphology of the $CuFe_{2-x}Ni_xO_4$ (x = 0, 0.1, 0.3, and 0.5) nanoparticles. The micrographs (Figure 3a–d) show predominantly spherical particles with a relatively uniform morphology across all compositions.

**Table 1.** Sample, Sample code, crystallite size, lattice parameter and energy gap of $CuFe_{2-x}Ni_xO_4$ (x = 0, 0.1, 0.3 & 0.5) nanoparticles.

| Sample | Sample code | Crystallite Size (nm) | Lattice Parameter (Å) | Energy gap (eV) |
|---|---|---|---|---|
| $CuFe_2O_4$ | a | 20 | 8.320 | 1.65 |
| $CuFe_{1.9}Ni_{0.1}O_4$ | b | 22 | 8.317 | 1.67 |
| $CuFe_{1.7}Ni_{0.3}O_4$ | c | 6 | 8.313 | 1.70 |
| $CuFe_{1.5}Ni_{0.5}O_4$ | d | 30 | 8.310 | 1.71 |

**Table 2.** Sample, Sample code, Rietveld refinement factors of $CuFe_{2-x}Ni_xO_4$ (x = 0.0, 0.1, 0.3 & 0.5) samples

| Sample | Sample code | $R_{wp}$ | $R_p$ | $R_e$ | S |
|---|---|---|---|---|---|
| $CuFe_2O_4$ | a | 6.62 | 5.27 | 6.17 | 1.07 |
| $CuFe_{1.9}Ni_{0.1}O_4$ | b | 7.49 | 5.93 | 7.04 | 1.06 |
| $CuFe_{1.7}Ni_{0.3}O_4$ | c | 8.81 | 6.16 | 5.58 | 1.58 |
| $CuFe_{1.5}Ni_{0.5}O_4$ | d | 5.96 | 4.69 | 4.92 | 1.21 |

© STM Journals 2026. All Rights Reserved 

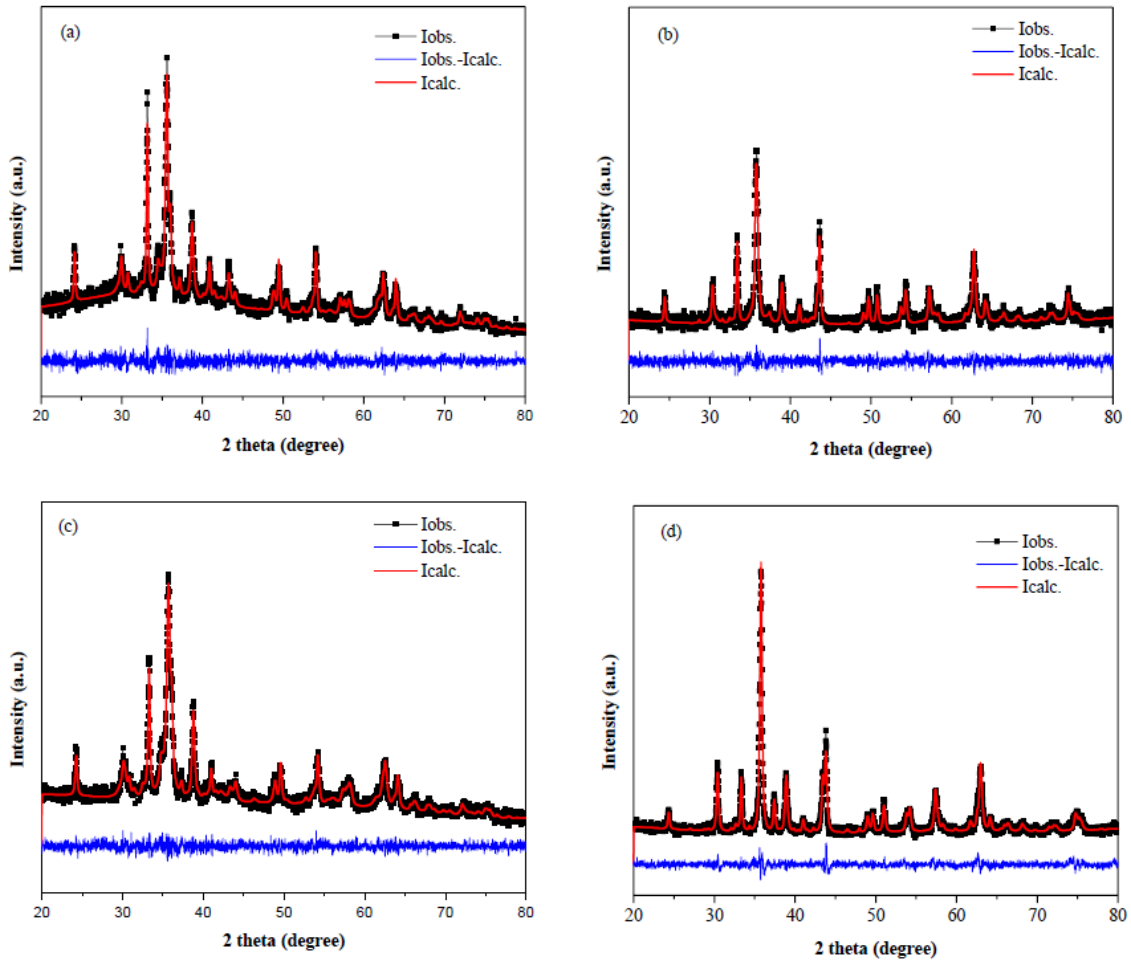


**Figure 2.** Rietveld refined XRD patterns of $CuFe_{2-x}Ni_xO_4$ (x = 0, 0.1, 0.3 & 0.5) nanoparticles.

Both the undoped and Ni-doped samples exhibit nanoscale particles that tend to form aggregated clusters, a characteristic behavior frequently observed in spinel ferrite nanoparticles due to strong magnetic dipole interactions and surface energy effects [23, 24].

Such aggregation is typical for ferrite nanostructures and may influence their dispersion capability when incorporated into polymer matrices. The observed morphology, characterized by fine particle size and clustered formations, is favorable for interfacial interactions within composite systems and can contribute to enhanced functional properties. Overall, the FE-SEM analysis provides valuable insights into the surface features and morphological evolution of the $CuFe_{2-x}Ni_xO_4$ nanoparticles, supporting their potential use as functional fillers in advanced polymer and hybrid composite applications [25].

**Energy-dispersive X-ray Spectroscopy (EDX) Analysis**

Energy-dispersive X-ray spectroscopy (EDX) was employed to analyze the elemental composition of the synthesized $CuFe_{2-x}Ni_xO_4$ ($0 \leq x \leq 0.5$) nanoparticles. The EDX spectra Figure 4 (a–b) provide qualitative and quantitative confirmation of the constituent elements in the $CuFe_2O_4$ and $CuFe_{1.5}Ni_{0.5}O_4$ samples. The detected peaks corresponding to Cu, Fe, Ni, and O validate the successful incorporation of $Ni^{2+}$ ions into the copper ferrite lattice without the presence of extraneous elements.

Elemental mapping further illustrates the spatial distribution of the constituent elements for both undoped and Ni-doped samples Figure 5 (a–c) and Figures 6 (a–d). For $CuFe_2O_4$, the maps show a uniform dispersion of Cu, Fe, and O, confirming the compositional homogeneity of the pristine ferrite.

© STM Journals 2026. All Rights Reserved 

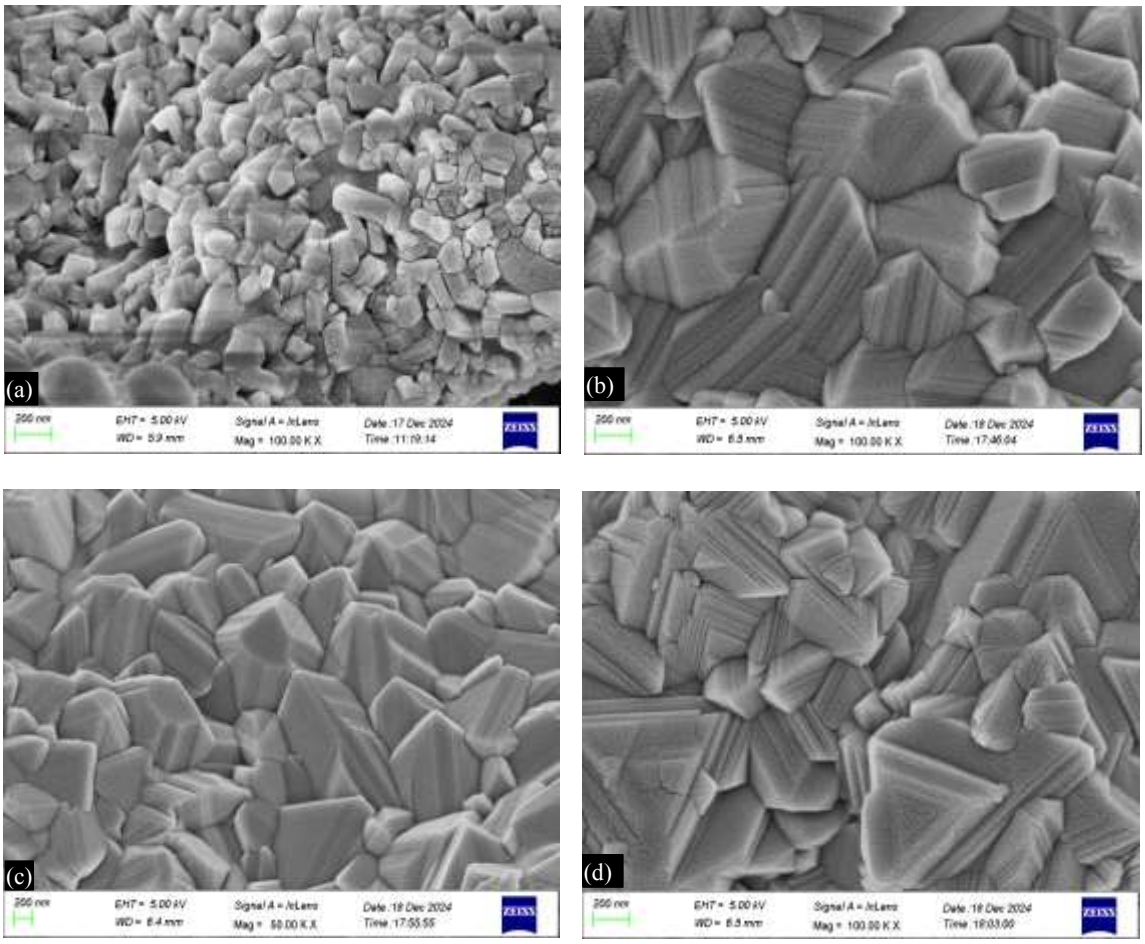


**Figure 3.** (a–d) FE-SEM image of $CuFe_{2-x}Ni_xO_4$ (x = 0, 0.1, 0.3 & 0.5) nanoparticles.

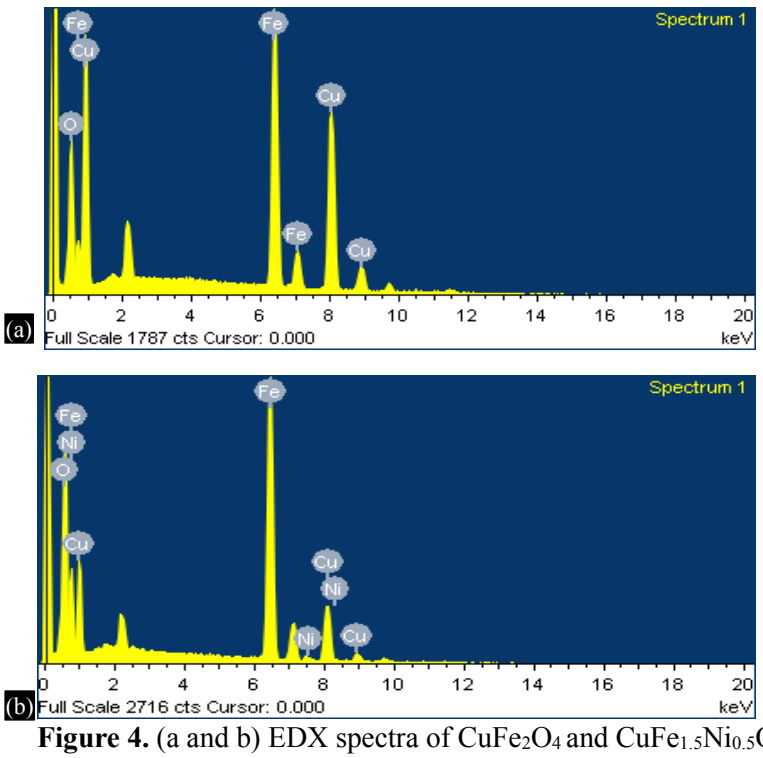


**Figure 4.** (a and b) EDX spectra of $CuFe_2O_4$ and $CuFe_{1.5}Ni_{0.5}O_4$ nanoparticles.
the $CuFe_2O_4$ structure [26].

© STM Journals 2026. All Rights Reserved 

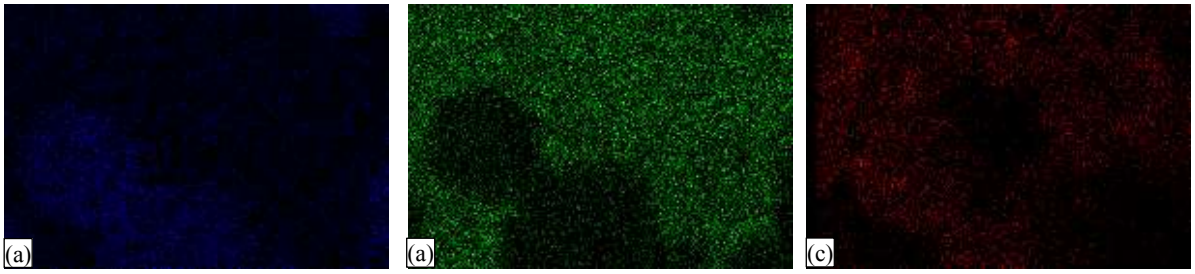


**Figure 5.** (a–c). Elemental Mapping spectra of $CuFe_2O_4$ nanoparticles.

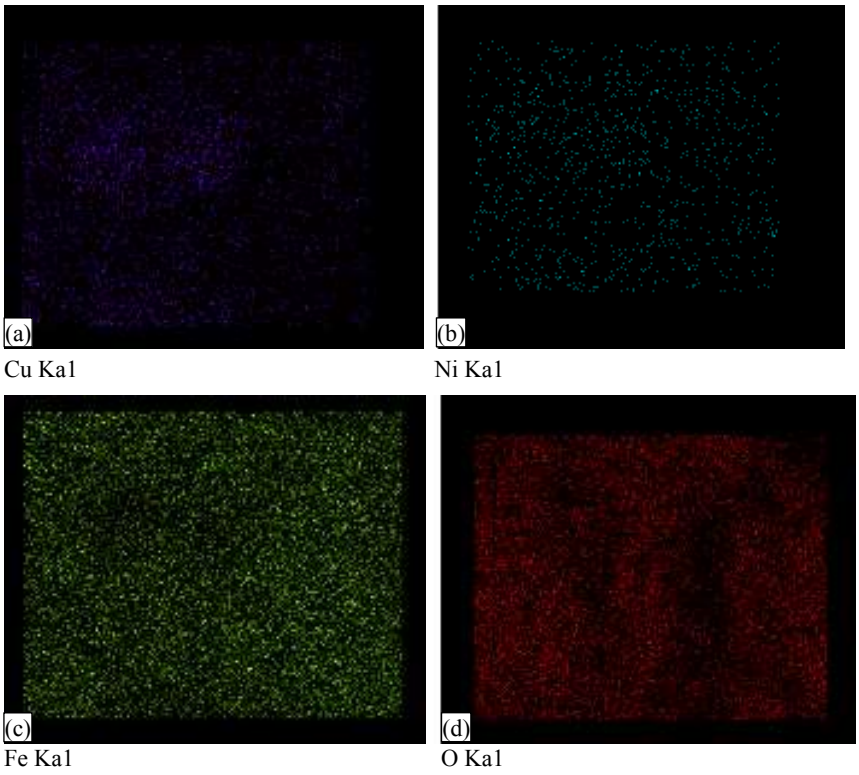


**Figure 6.** (a-d) Mapping spectra of $CuFe_{1.5}Ni_{0.5}O_4$ nanoparticles.

In the Ni-substituted sample (x = 0.5), the elemental maps indicate an even and well-distributed presence of Ni along with Cu, Fe, and O throughout the nanoparticle clusters. This uniform distribution demonstrates the effective incorporation of Ni into the spinel structure.

The consistent elemental dispersion observed across all compositions supports the successful synthesis of the $CuFe_{2-x}Ni_xO_4$ nanoparticles and reinforces the structural integrity of the cubic spinel phase [26]. Such homogeneity is essential for ensuring reliable functional behavior, especially when these nanoparticles are utilized as fillers in polymer and hybrid composite materials.

**UV-Visible Analysis**

By applying the Tauc relation, which uses the Kubelka-Munk function to translate reflectance data into absorption coefficients [27], as provided by Equation (3), the band gap of $CuFe_{2-x}Ni_xO_4$ (x = 0, 0.1, 0.3, and 0.5) nanoparticles was obtained:

$$\alpha = F(R) = \frac{(1-R)^2}{2R} \quad (3)$$

© STM Journals 2026. All Rights Reserved 

where α is the absorption coefficient, and F(R) represents the Kubelka-Munk function. The Taucrelation, given by Equation (4), is:

$$F(R)h\nu = A(h\nu - E_g)^n \quad (4)$$

where n = 1/2 and n = 2 correspond to allowed direct and indirect electronic transitions, respectively, leading to the calculation of direct and indirect band gaps [28,29].

Figure 7 displays the Tauc plots of $(F(R)h\nu)^2$ versus photon energy (hν) for the $CuFe_{2-x}Ni_xO_4$ nanoparticles (x = 0, 0.1, 0.3, and 0.5). The optical band gap values were obtained by extrapolating the linear portion of each curve to the energy axis. The estimated band gaps for the respective compositions are 1.65 eV, 1.67 eV, 1.70 eV, and 1.71 eV, indicating a gradual increase in band gap with higher Ni content. This systematic shift in band gap can be attributed to modifications in the electronic structure arising from Ni substitution, as well as size-dependent effects commonly observed in nanoscale ferrite systems. The variation reflects the influence of altered cation distribution and reduced crystallite size, which together contribute to enhanced quantum confinement. Such tunability in optical behavior is advantageous for tailoring these ferrite nanoparticles for optoelectronic, photocatalytic, and polymer-based composite applications where controlled light absorption is essential [30].

**FTIR Analysis**

The vibrational characteristics of the $CuFe_{2-x}Ni_xO_4$ ($0 \leq x \leq 0.5$) nanoparticles were examined using Fourier-transform infrared (FTIR) spectroscopy in the range of 400–4000 $cm^{-1}$ to identify the functional groups and confirm the formation of metal–oxygen bonds within the spinel lattice [31]. The FTIR spectra presented in Figure 8 exhibit several characteristic peaks corresponding to both lattice vibrations and surface functional groups.

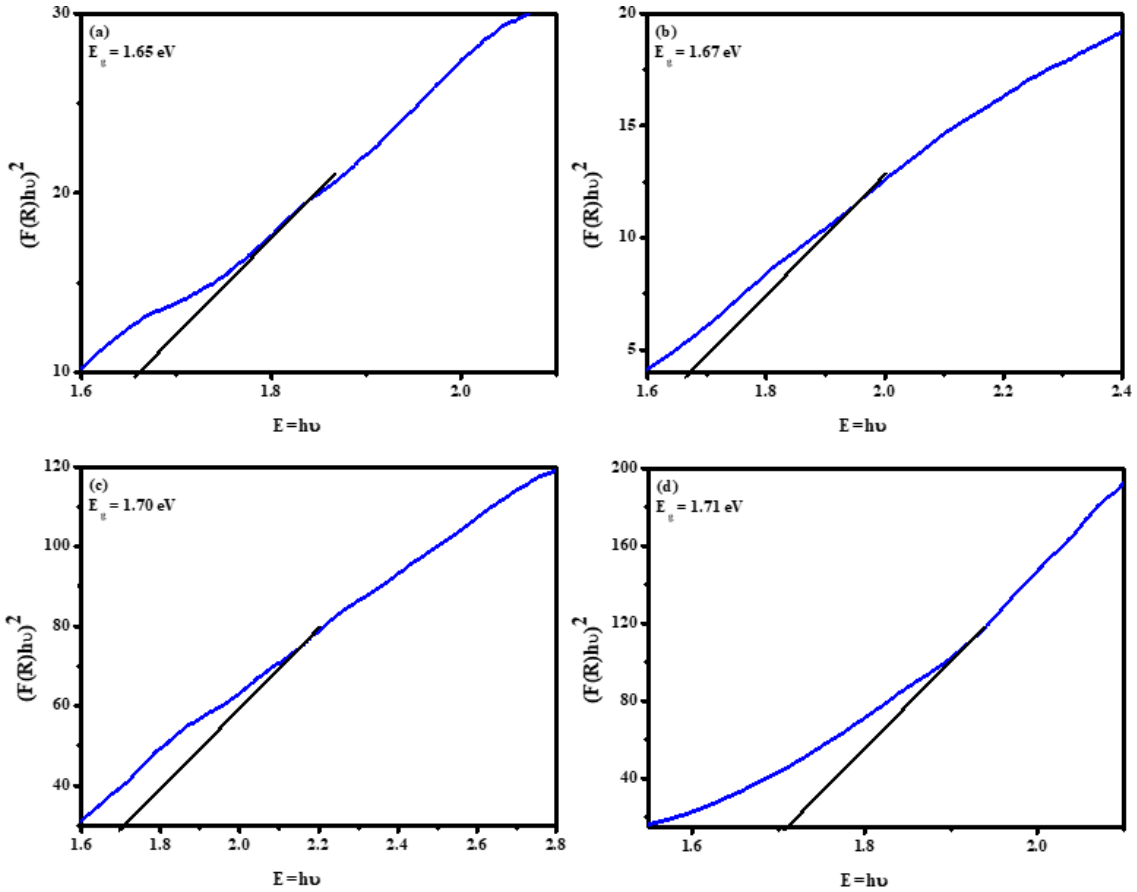


**Figure 7.** Band gap spectra of $CuFe_{2-x}Ni_xO_4$ (x = 0, 0.1, 0.3 & 0.5) nanoparticles.

© STM Journals 2026. All Rights Reserved 

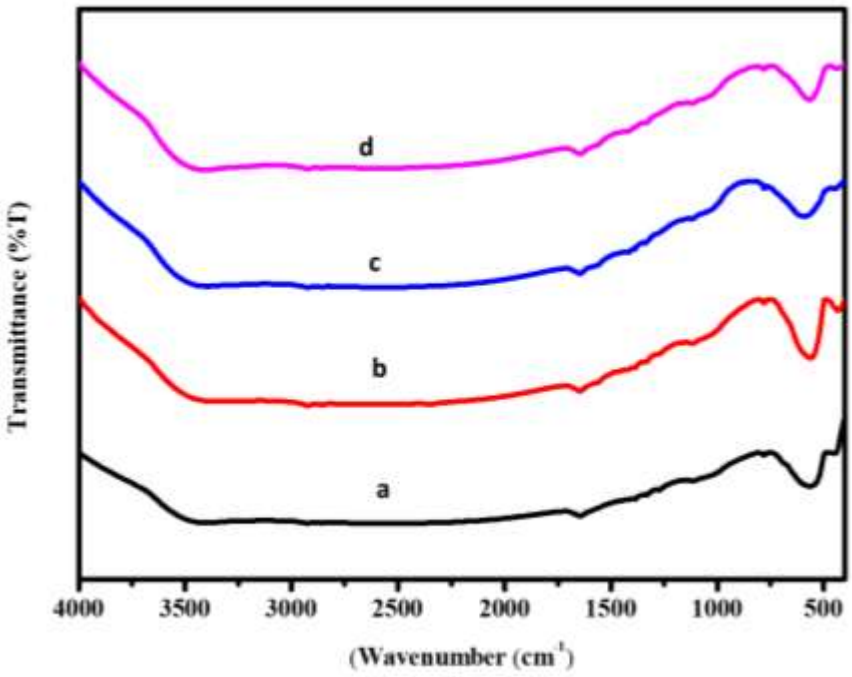


**Figure 8.** FTIR spectra of $CuFe_{2-x}Ni_xO_4$ (x = 0, 0.1, 0.3 & 0.5) nanoparticles.

Distinct absorption bands observed at 578 $cm^{-1}$ and 437 $cm^{-1}$ are attributed to the intrinsic metal–oxygen stretching vibrations associated with the tetrahedral (Fe–O/Cu–O) and octahedral (Fe–O) sites of the spinel structure, respectively [32,33]. The presence of these bands confirms the successful formation of the $CuFe_{2-x}Ni_xO_4$ spinel phase across all compositions. The slight shifts in these vibrational modes with increasing Ni content indicate modifications in the local cation environment due to the substitution of $Cu^{2+}$ by the smaller $Ni^{2+}$ ions, leading to subtle variations in bond strength and lattice distortions.

Additionally, several peaks located at 3781, 3441, 2854, 2329, 1744, 1644, 1562, 1459, and 1337 $cm^{-1}$ correspond to stretching and bending vibrations of surface hydroxyl (–OH) groups and adsorbed water molecules. These features are commonly observed in ferrite nanoparticles due to their high surface area and strong affinity for ambient moisture. Peaks in the higher wavenumber region (1112–850 $cm^{-1}$) may also arise from residual organic species originating from the precursor or combustion fuel, indicating partial surface functionalization. The observed variations in peak intensities and positions with Ni substitution suggest that Ni incorporation influences the vibrational dynamics of the spinel lattice. Such structural modifications can affect the dielectric and interfacial polarization behavior of the nanoparticles, which are critical parameters when these materials are used as fillers in polymer and hybrid composites [34].

## CONCLUSIONS

The combustion method was successfully employed to synthesize $CuFe_{2-x}Ni_xO_4$ ($0 \leq x \leq 0.5$) nanoparticles, yielding a single-phase spinel structure with a cubic crystal system. X-ray diffraction (XRD) confirmed phase purity, and crystallite sizes were estimated using the Debye–Scherrer approach. Energy-dispersive X-ray spectroscopy (EDX) verified the presence of Cu, Ni, Fe, and O elements in the synthesized powders. Diffuse reflectance UV–Vis spectroscopy revealed optical band gaps in the range of 1.65 – 1.71 eV, indicating tunable electronic transitions with Ni substitution. FE-SEM images showed spherical to flake-like morphologies, supporting uniform particle formation suitable for composite dispersion. FT-IR spectra further confirmed characteristic metal–oxygen vibrations (Cu–O and Fe–O) associated with the spinel lattice. Moreover, the structural, optical, and morphological

© STM Journals 2026. All Rights Reserved 

features demonstrate that $CuFe_{2-x}Ni_xO_4$ nanoparticles possess desirable functional characteristics for use as active fillers in polymer and composite systems. Their tunable band gap and stable spinel framework make them promising for electromagnetic shielding materials, polymer–ferrite hybrid devices, and multifunctional composite applications. Future studies may focus on integrating these ferrites into polymer matrices to evaluate interfacial compatibility, mechanical enhancement, and multifunctional performance within advanced composite architectures.

**REFERENCE**

1. Acharya P, Desai R, Aswal VK, et al. Structure of Co–Zn ferrite ferrofluid: a small angle neutron scattering analysis. J. Phys. 2008; 71: 1069–1074p.
2. Emadi H., Mobarak H. Synthesis and characterization of copper ferrite nanoparticles and its application as MRI contrast agent. Lett. Appl. Nano Bio Sci. 2019; 8(1): 541–544p.
3. Yue Z, Zhou J, Li L, et al. Effect of copper on the electromagnetic properties of Mg–Zn–Cu ferrites prepared by sol–gel auto-combustion method. Mater. Sci. Eng. B. 2001; 86(1): 64–69p.
4. Srikanth K, Nutalapati V. Copper ferrite nanoparticles induced cytotoxicity and oxidative stress in Channel catfish ovary cells. Chemosphere. 2022; 287: 132166p.
5. Gautam S, Charak R, Garg S, et al. Tailoring magnetism in chromium-doped zinc cobalt ferrite nanostructure for advanced spintronic memory devices. Mater. Today Chem. 2024; 41: 102291p.
6. Alqassem B, Banat F, Palmisano G, et al. Emerging trends of ferrite-based nanomaterials as photocatalysts for environmental remediation: A review and synthetic perspective. Sustain. Mater. Technol. 2024; e00961p.
7. Masunga N, Mamba BB, Getahu YW, et al. Synthesis of single-phase superparamagnetic copper ferrite nanoparticles using an optimized coprecipitation method. Mater. Sci. Eng. B 2021; 272: 115368p.
8. Sundararajan M, Kennedy LJ, Vijaya JJ, et al. Microwave combustion synthesis of $Co_{1-x}Zn_xFe_2O_4$ ($0 \leq x \leq 0.5$): Structural, magnetic, optical and vibrational spectroscopic studies. Spectrochim. Acta A Mol. Biomol. Spectrosc. 2015; 140: 421–430p.
9. Mathew D.S., Juang R.S. An overview of the structure and magnetism of spinel ferrite nanoparticles and their synthesis in microemulsions. Chem. Eng. J. 2007; 129(1–3): 51–65p.
10. Noreen S, Hussain A. Structural, optical, morphological and magnetic properties of $Cu_{0.25}M_{0.75}Fe_2O_4$ (M = Mn, Mg, Ni and Co) ferrites for optoelectronic applications. Opt. Mater. 2023; 139: 113797p.
11. Masunga N, Mamba BB, Kefeni KK. Improved magnetic, optical, electrochemical, and structural properties of copper ferrite through optimized addition of samarium dopant using the co-precipitation method. Mater. Sci. Eng. B 2023; 296: 116662p.
12. Gingaşu D, Mîndru I, Patron L, Carp O, et al. Copper ferrite obtained by two “soft chemistry” routes. J. Alloys Compd. 2006; 425(1–2): 357–361p.
13. Karakaş ZK. A comprehensive study on the production and photocatalytic activity of copper ferrite nanoparticles synthesized by microwave-assisted combustion method as an effective photocatalyst. J. Phys. Chem. Solids 2022; 170: 110927p.
14. Meng X, Xu W, Ren X, et al. Progress and challenges of ferrite matrix microwave absorption materials. Materials 2024; 17(10): 2315p.
15. Sukumar M, Rajabathar JR, Lohedan HAL, et al. Synthesize and characterization of copper doped nickel ferrite nanoparticles effect on magnetic properties and visible light catalysis for rhodamine dye degradation mechanism. J. Alloys Compd. 2023; 953: 169902p.
16. Bashaa DB, Dahiyaa D, Veena E. Dielectric and magnetic properties of zinc copper ferrite nanoparticles. J. Ovonic Res. 2021; 17(6): 589–594p.
17. Sundararajan M, Kennedy LJ, Aruldoss U, et al. Microwave combustion synthesis of zinc substituted nanocrystalline spinel cobalt ferrite: Structural and magnetic studies. Mater. Sci. Semicond. Process. 2015; 40(1): 1–10p.
18. Revathi R, Sukumar M, Kumar A, et al. Facile synthesis of $Ni^{2+}$-doped $MgFe_2O_4$ spinel nanoparticles: Structural, optical, magnetic, and dielectric behavior. J. Inorg. Organomet. Polym. 2024; 34: 374–386p.

© STM Journals 2026. All Rights Reserved 

19. Patterson AL. The Scherrer formula for X-ray particle size determination. Phys. Rev. 1939; 56(10): 978–982p.
20. Razik NA. Precise lattice constants determination of cubic crystals from x-ray powder diffractometric measurements. Appl. Phys. A 1985; 37: 187–189p.
21. Dhiwahar AT, Sundararajan M, Sakthivel P, et al. Microwave-assisted combustion synthesis of pure and zinc-doped copper ferrite nanoparticles: Structural, morphological, optical, vibrational, and magnetic behavior. J. Phys. Chem. Solids 2019; 138: 109257p.
22. Abbas YM, Mansour SA, Ibrahim MH, et al. Microstructure characterization and cation distribution of nanocrystalline cobalt ferrite. J. Magn. Magn. Mater. 2011; 323(22): 2748–2756p.
23. Mahajan H, Godara SK, Srivastava AK. Synthesis and investigation of structural, morphological, and magnetic properties of manganese-doped cobalt–zinc spinel ferrite. J. Alloys Compd. 2022; 896: 162966p.
24. Noreen S, Hussain A. Structural, optical, morphological and magnetic properties of $Cu_{0.25}M_{0.75}Fe_2O_4$ (M = Mn, Mg, Ni and Co) ferrites for optoelectronic applications. Opt. Mater. 2023; 139: 113797p.
25. Baskar S, Yuvaraj S, Sundararajan M, et al. Influence of $Ca^{2+}$ ion substitution on structural, morphological, optical, thermal and magnetic behaviour of $Mg_{1-x}Ca_xFe_2O_4$ ($0 \leq x \leq 0.5$) spinel. J. Supercond. Nov. Magn. 2020; 33: 3949–3956p.
26. Sundararajan M, Kennedy LJ, Vijaya JJ, et al. Microwave combustion synthesis of $Co_{1-x}Zn_xFe_2O_4$ ($0 \leq x \leq 0.5$): Structural, magnetic, optical and vibrational spectroscopic studies. Spectrochim. Acta A Mol. Biomol. Spectrosc. 2015; 140(1): 421–430p.
27. Sundararajan M, Sukumar M, Dash CS, et al. A comparative study on $NiFe_2O_4$ and $ZnFe_2O_4$ spinel nanoparticles: Structural, surface chemistry, optical, morphology and magnetic studies. Physica B Condens. Matter 2022; 644: 414232p.
28. Rosa JC, Segarra M. Optimization of the synthesis of copper ferrite nanoparticles by a polymer-assisted sol–gel method. ACS Omega 2019; 4(19): 18289–18298p.
29. Subhashini N, Revathi S, Ubaidullah M, et al. $Gd^{3+}$ substituted $BiFeO_3$ perovskite nanoparticles: facile synthesis, characterization and applications in heterogeneous catalysis. Dalton Trans. 2023; 52: 2735p.
30. Sundararajan M, Kennedy LJ. Photocatalytic removal of rhodamine B under visible light using $Co_{1-x}Cu_xFe_2O_4$ ($0 \leq x \leq 0.5$) nanoparticles. J. Environ. Chem. Eng. 2017; 5(4): 4075–4092p.
31. Mathankumar K, Sukumar M, Dash CS, et al. Facile synthesis, characterization, catalytic and photocatalytic activity of multiferroic $BiFeO_3$ perovskite nanoparticles. J. Inorg. Organomet. Polym. 2022; 32: 3476–3487p.
32. Chatterjee BK, Bhattacharjee K, Dey A, et al. Influence of spherical assembly of copper ferrite nanoparticles on magnetic properties: orientation of magnetic easy axis. Dalton Trans. 2024; 43: 7930–7944p.
33. Tedjieukeng HMK, Tsobnang PK, Fomekong RL, et al. Structural characterization and magnetic properties of undoped and copper-doped cobalt ferrite nanoparticles prepared by the octanoate coprecipitation route at very low dopant concentrations. RSC Adv. 2018; 8: 38621–38630p.
34. Kherrouba N, Bouamer A. Magnetic, optical, structural and thermal properties of copper ferrite nanostructured synthesized by mechanical alloying. Micro Nano Lett. 2021; 16(4): 251–256p.

© STM Journals 2026. All Rights Reserved 